Applied Surface Science 459 (2018) 318–326

Contents lists available at ScienceDirect

Applied Surface Science

journal homepage: www.elsevier.com/locate/apsusc

Full Length Article

Adsorption of polythiophene/TiO_2 composite for Zn (II), Pb (II) and Cu (II): Selectivity and synergistic effect investigation

Jie Chen, Lin Zhang, Jinwei Zhu, Ning Wang, Jiangtao Feng*, Wei Yan*

Department of Environmental Science and Engineering, State Key Laboratory of Multiphase Flow in Power Engineering, Xi'an Jiaotong University, Xi'an 710049, PR China

ARTICLE INFO

Keywords:
Polythiophene/TiO_2 composite
Self-doping
Synergistic effect
Selective adsorption
Mechanism investigation

ABSTRACT

A composite with self-doping nature, polythiophene (PTh)/TiO_2 with impressive selectivity was synthesized in the aqueous medium to support the mechanism on synergistic effect between PTh and TiO_2. An interesting self-doping of $TiO_2(O^-)$ on the polythiophene in the $PTh^+/TiO_2(O^-)$ composite was also prepared with tunable heterojunction structure by adjusting the solution pH. An impressive selective adsorption property with an ascending order of $Zn^{2+} > Pb^{2+} \gg Cu^{2+}$ was achieved in the single and competitive adsorption study, where the adsorption for Cu^{2+} could be almost suppressed. This interesting selective adsorption was confirmed to be caused by the dedoping of $TiO_2(O^-)$ in the heavy metal ion solution due to the metastable doping form of PTh in non-acid solution from the TGA and electrochemical point of view. While the selective adsorption of the composite was also determined on TiO_2. The general mechanisms on synergistic effect and on selective adsorption were successfully convinced through the designed experiment, providing some reliable guidelines for designing adsorbents with selectivity towards specific heavy metal ions. In addition, $PTh^+/TiO_2(O^-)$ composite with high adsorption capacity for Zn^{2+} and Pb^{2+} can be readily applied in the practical application, especially in the Cu^{2+} rich waste water without capacity loss.

1. Introduction

Adsorption is a low-cost industrial separation technique for the treatment of heavy metal ion-containing effluents, and it is particularly effective when adsorbents with high adsorption capacity and selectivity are applied [1,2]. Recent studies have focused on many interesting adsorbents such as fly ash [3], graphene oxide and reduced graphene oxide [4], dead biomass [5], inorganic minerals [6], molecular compounds with different functional groups [1], and so on. However, multiple heavy metal ions normally co-exist in natural and industrial water environment, and adsorption capacity of these adsorbents is still not high enough, especially in the wastewater where the ions compete with each other for the adsorption sites [2]. Therefore, finding new materials and methods for fabricating adsorbents with high adsorption performance and selectivity remains challenging.

In this case, integrating a synthetic polymer and an inorganic mineral to produce a unique organic/inorganic composite type adsorbent have received growing investigation interest in recent years due to their synergistic effect in the composite [7]. A chitosan based composite adsorbent with clay was synthesized and found the interesting synergistic effect on the adsorption for binary mixtures of Pb (II) and Cd (II) from water [8]. Lignosulfonate-graphene oxide-polyaniline (LS-GO-PANi) composite was applied for Pb (II) adsorption and suggested that the synergistic phenomena between PANi and LS-GO plays a key role in the adsorption [9]. A similar synergistic effect is also found in our previous work [10–13]. Even though the synthesis of composites is of great interest in the adsorbent synthesis, little investigation has been paid on the mechanism of the synergistic effect between the components in a composite, leaving the mechanism still unknown. Without the guidance of the mechanism, it would greatly restrict the development of the design and synthesis for the composite adsorbents.

In another important aspect, in order to prepare adsorbent with interesting selectivity, different types of conjugated polymers and inorganic metal oxides have been used. Specifically, metal oxides have demonstrated a special selective adsorption affinity to some heavy metal ions, such as ferric oxides toward Pb (II) [14], manganic oxides possess to Cu (II) [15], Zn(II) on silicic oxides, and many more [16]. While the conjugated polymer of polypyrrole, polyaniline and polythiophene are promising candidates for the synergistic effect due to their novel conjugated structure and tunable electrochemical properties concerning the ion doping-dedoping process in the solution with different pH (Scheme 1) [17]. Even though there has been some published literature concerning polymer/metal oxides for heavy metal adsorption, there have been limited investigation on adsorption in multiple metal

* Corresponding authors.
E-mail addresses: fjtes@xjtu.edu.cn (J. Feng), yanwei@xjtu.edu.cn (W. Yan).

https://doi.org/10.1016/j.apsusc.2018.08.008
Received 25 April 2018; Received in revised form 20 July 2018; Accepted 1 August 2018
Available online 02 August 2018
0169-4332/

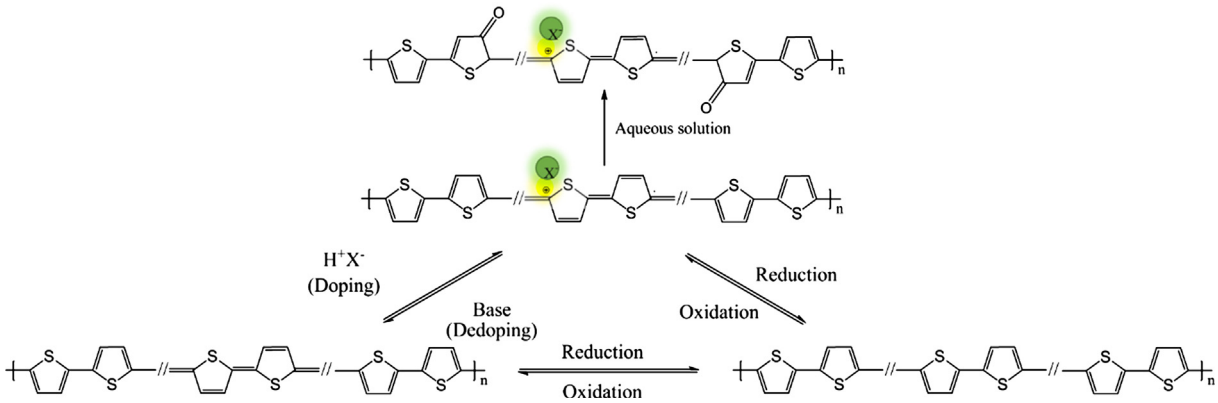

Scheme 1. Interconversions between the various redox states in PPy (a polaron exists in six thiophene rings).

ion solution to take the selectivity of adsorption into consideration.

The aim of this study is synthesis of polythiophene (PTh)/TiO_2 composite to get insight into the mechanism on the synergistic effect between polymer and metal oxide, and on the selectivity for specific heavy metal ion. Herein, the self-doping nature of the PTh/TiO_2 was characterized and discussed. Three important hazardous ions including Pb (II), Zn (II) and Cu (II) were employed as the experimental targets and applied in the single and competitive adsorption process to reveal the selective adsorption property of PTh/TiO_2 composite.

2. Experimental

2.1. Materials

Thiophene used in this study was purchased from TCI (Shanghai) Development Co., Ltd and used as received. The other chemicals used in this study were all purchased from Sinopharm Chemical Reagent Co., Ltd (China). All chemicals were analytical grade. The standard heavy metal solutions used in the study were prepared using $Pb(NO_3)_2$, $Cu(NO_3)_2{\cdot}3H_2O$ and $Zn(NO_3)_2{\cdot}6H_2O$, respectively with deionized water.

2.2. Synthesis of the PTh, TiO_2 and PTh/TiO_2 composite

The synthesis of the adsorbents was carried out in a 500 mL three-jacketed glass reactor with a mechanical stirrer. 0.8 mL of HNO_3 was slowly added in 400 mL of deionized water to prepare the acid solution for better polymerization of thiophene (Caution! The HNO_3 is highly corrosive!). 20 mL of titanium (IV) isopropoxide (0.066 mol) was dropwise injected into 400 mL of deionized water in the flask and stirred for 60 min to prepare the TiO_2 suspension solution. Then 3.6 mL of thiophene (0.05 mol) was added in and stirred for 60 min to make sure the thiophene can be totally adsorbed on the TiO_2 [18,19]. 20.704 g of ammonium peroxodisulfate (APS, 0.1 mol) was subsequently placed into the solution, and start heating to 50 °C in the meantime (Caution! The ammonium peroxodisulfate is corrosive!). The reaction was kept at 50 °C with whisking for 24 h. Finally, the obtained powder was filtrated and dried at 50 °C for 24 h. The TiO_2 and PTh, which is compared in the investigation, were also synthesized with the same procedure without thiophene monomer and ammonium peroxodisulfate or TiO_2 adding. The yield of PTh was 53.47%; the yield of PTh/TiO_2 was 92.69%.

2.3. Characterization instruments

The Fourier transform infrared spectra (FT-IR) of PTh, TiO_2 and PTh/TiO_2 composite were obtained on a BRUKER TENSOR 37 FT-IR spectrometer by the KBr pellet method. The thermogravimetric analysis (TGA) was performed on a Setaram Labsys Evo in N_2 flow with the heating rate of 10 °C/min. The zeta potential investigations were conducted on a Malvern Zetasizer Nano ZS90. X-ray diffraction (XRD) patterns were acquired on an X'Pert PRO Diffractometer, and the experimental range was set within 10–80°with wavelength of 1.5406 Å using Cu-Kα radiation method. N_2 adsorption and desorption isotherms were recorded on a Builder SSA-4200 at 77 K. The specific surface area is calculated using the multiple point BET method, and total pore volume and average pore radius were calculated based on the BJH method (using the desorption branch). The scanning electron microscopy (SEM) was performed on a JSM-6700F to investigate the morphology of sample. Transmission electron microscopy images (TEM) were recorded on a JEM model 2100 electron microscope. An inductive coupled plasma emission spectrometer of Shimadzu ICPE-9000 was applied to determine the concentration of the heavy metal ions.

2.4. Adsorption experiments

In the experiments in Section 3.2, the volume of the heavy metal solution was kept at 20 mL, and the dose of the adsorbent was kept at 2 g/L. A shaker with controllable temperature was occupied, and the agitation speed was kept at 200 rpm. To eliminate the precipitation of metal ions, the solution pH was kept at 5.

In the kinetic experiment, 400 mg/L Pb^{2+}, Zn^{2+} and Cu^{2+} solutions were applied respectively in various contact time from 0 to 180 min in a single-ion system. In the single-ion isotherm study, various initial concentration of Pb^{2+}, Zn^{2+} and Cu^{2+} solutions were applied respectively at 25, 35 and 45 °C for 3 h. For Pb^{2+} adsorption, the initial concentration was kept at 100, 200, 300, 400, 600 and 800 mg/L, respectively; For Zn^{2+} and Cu^{2+}adsorption, the initial concentration was kept at 10, 50, 100, 200, 400 and 600 mg/L, respectively. In the multiple-ion isotherm study, the Pb^{2+}, Zn^{2+} and Cu^{2+} mixed solution with initial concentration of 50, 100, 200, 300, 400 mg/L, respectively were investigated at 25 °C for 3 h. In the effect of pH experiment, the initial concentration of 200 mg/L heavy metal ion solution with initial pH from 1 to 5 were used. The pH was carefully adjusted using concentrated HNO_3 and NaOH solution (Caution! The HNO_3 and NaOH are highly corrosive!). The initial concentration was all kept as 400 mg/L. As for the calculation, the adsorption capacity and recycle efficiency was calculated as follows:

$$Q_e = \frac{(C_0 - C_e)V}{m} \tag{1}$$

$$\text{Recycleefficiency} = \frac{Q_{e,n}}{Q_{e,0}} \times 100\% \tag{2}$$

where Q_e (mg/g) is the equilibrium adsorption capacity; C_0 and C_e (mg/L) are the initial and equilibrium concentrations of heavy metal ions, respectively; m (g) is the weight of adsorbent; V (mL) is the solution volume; $Q_{e,0}$ and $Q_{e,n}$ is the adsorption capacity at the initial and at n cycle.

Table 1
Assignments of the FT-IR absorptions for the PTh, TiO_2 and PTh/TiO_2 composite before and after adsorption with Pb^{2+}, Zn^{2+} and Cu^{2+} [21].

Frequencies (cm^{-1})												Assignments
Before adsorption			After adsorption									
TiO_2	PTh	PTh/TiO_2	PTh/TiO_2 Pb	PTh/TiO_2 Zn	PTh/TiO_2 Cu	TiO_2 Pb	TiO_2 Zn	TiO_2 Cu	PTh Pb	PTh Zn	PTh Cu	
3412	–	3353	3387	3202	3410	3519	3547	3436	–	–	–	-OH stretching vibration
–	1676	Overlapped	Overlapped	Overlapped	Overlapped	–	–	–	1669	1675	1673	—C=O or C=C in thiophene ring
1629	–	1636	1621	1622	1628	1621	1619	1625	–	–	–	-OH in-plane bending vibration
–	1554	1552	1552	1553	1554	–	–	–	1554	1554	1554	C=C symmetric stretching
–	1407	1407	1407	1407	1407	–	–	–	weak	weak	1417	C—C stretching vibration
–	–	–	1380	1380	1380	1380,1375	1380,1375	1380	1380	1380	1380	NO_3^-
–	1211					–			1211			SO_4^{2-}
–	1156, 786					–	–	–	1156, 786			C—H aromatic vibration
–	1029,665	994,652	995,966,624	983, 655	988,641	–	–	–	1042,661	1035,662	1046,657	C-S vibration
–	–	–	–	–	834	–	–	834	–	–	834	Cu^{2+}
–	–	–	–	828	–	–	828	–	–	828	–	Zn^{2+}
–	–	–		–	–	720	–	–	720	–	–	Pb^{2+}
400–700	–	400–700	400–700	400–700	400–700	400–700	400–700	400–700	–	–	–	O–Ti–O

3. Results and discussion

3.1. Characterization

Herein, PTh and PTh/TiO_2 composite are synthesized through a radical polymerization process using APS as an oxidation agent. At the initial of the process, thiophene monomers are adsorbed on the surface of TiO_2, followed by the polymerization by the oxidant APS that could remove one electron from each thiophene monomer through forming a radical sulfate, which is similar to the polymerization of pyrrole [18,19]. The formed PTh and PTh/TiO_2 composite are illustrated using FTIR spectra shown in Table 1 and Fig. S1. It can be noted some of the characteristic peaks assigned to PTh are weak in the spectrum of the composite, which may due to the overlap of strong peaks ascribed to TiO_2. In addition, the loading rate of PTh may be relatively lower when the reaction is conducted in the aqueous medium due to the influence of OH^- [20]. Anyhow, the typical peaks situated at around 1676, 1554, 1407, 988 and 641 cm^{-1} assigned to polythiophene [21] and at 400–700 cm^{-1} attributed to TiO_2 [22] can be still detected in the spectrum of PTh/TiO_2 composite, confirming the successful loading of PTh onto TiO_2. It is notable to observe the peaks at 1676 cm^{-1} could also be assigned to C=O in the spectrum of PTh, suggesting that the PTh prepared by using the synthesis method in the aqueous solution is a polythiophene derivative. Specifically, several investigations indicated that the polymerization of the heterocyclic compounds such as pyrrole and thiophene is very easy to be influenced by the nucleophilic OH^-, and form the C=O on the β-C [23]. The PTh synthesized in the chloroform is hydrophobic, and the hydrophobic property could influence the contact and interaction between the PTh and heavy metal ions in the wastewater. Therefore, introduction of C=O would improve the hydrophily of the PTh and improve the interaction between PTh and heavy metal ions, exhibiting the advantage of the method we proposed for the PTh polymerization.

Supplementary data associated with this article can be found, in the online version, at https://doi.org/10.1016/j.apsusc.2018.08.008.

The conceivable structure of the synthesized PTh/TiO_2 composite is illustrated in Scheme 1. This structure is carefully illustrated from the characterization result and literature review, and a polaron is supposed to exist in six thiophene ring because the length of the conjugated rings are suggested to be quite short due to the interruption of the C=O

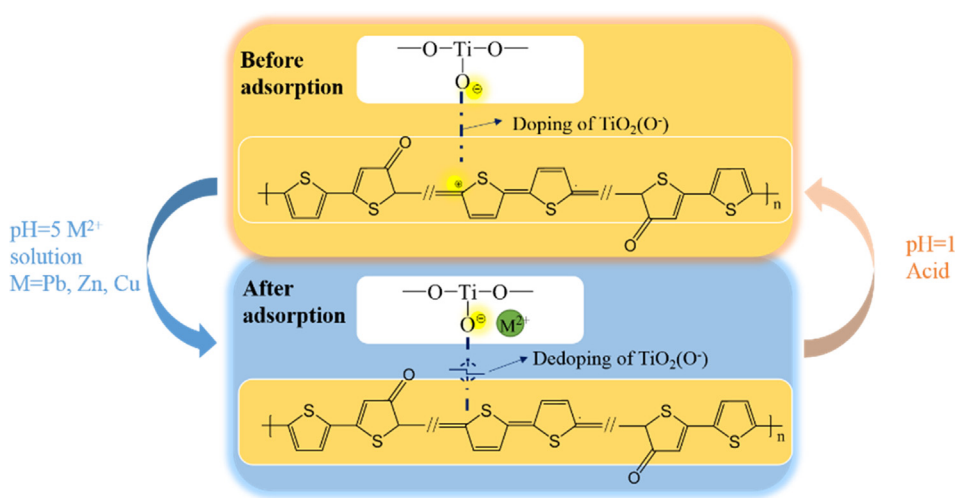

Scheme 2. The synergistic adsorption between PTh and TiO_2 in the $PTh^+/TiO_2(O^-)$ composite for the selective adsorption for heavy metal ions.

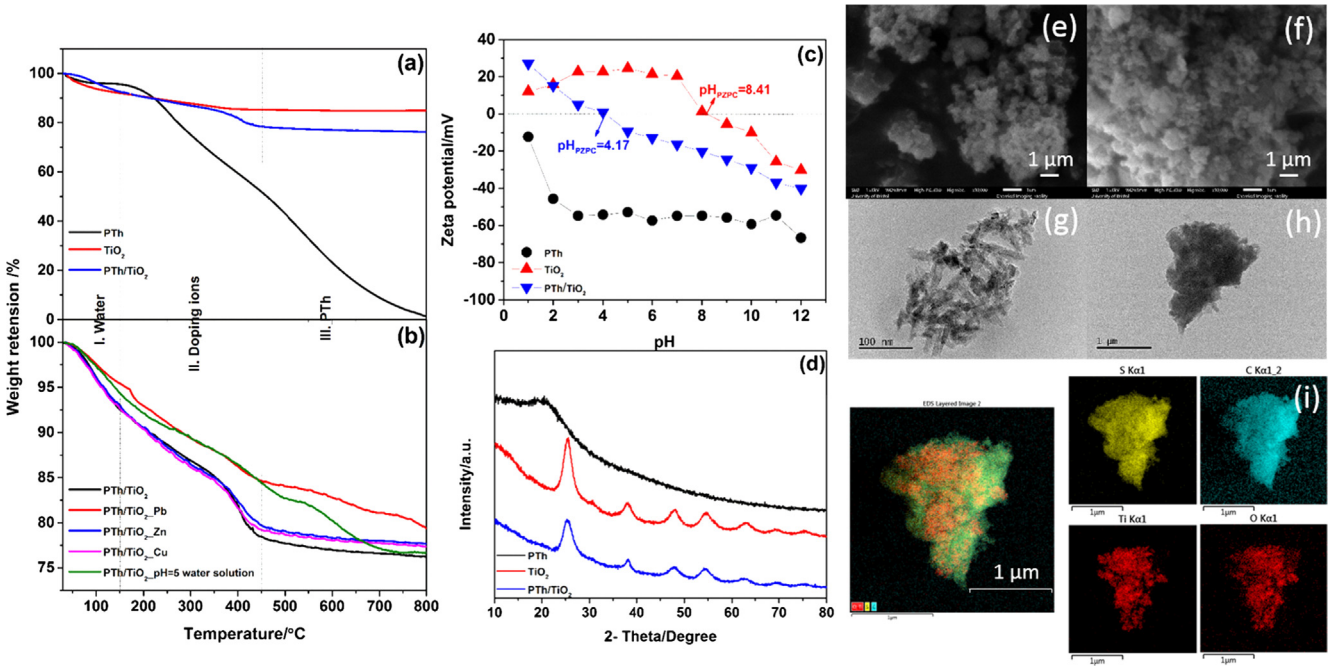

Fig. 1. Characterization of PTh/TiO_2 composite: TG analysis of PTh, TiO_2 and PTh/TiO_2 composite before (a) and after (b) adsorption of Pb^{2+}, Zn^{2+} and Cu^{2+}; Zeta potentials of PTh, TiO_2 and PTh/TiO_2 composite in different pH solution (c); XRD spectra of PTh, TiO_2 and PTh/TiO_2 composite (d); SEM, TEM images of TiO_2 (e, g) and PTh/TiO_2 composite (f, h); TEM-EDS images of PTh/TiO_2 composite (i).

group in the chain [24–29]. On the other hand, the peaks ascribed to –OH at 3412 and 1629 cm^{-1} in the spectrum of TiO_2 and at 1029 and 665 cm^{-1} attributed to C-S in the spectrum of PTh shift in the spectrum of PTh/TiO_2 composite, which is also observed in the study of PTh/titania nanotube composite [30,31], confirming the hypothesis on the interaction between PTh and TiO_2 in the composite that TiO_2 with hydroxyl ($TiO_2(O^-)$) plays as a dopant doping into the PTh chain. From the FTIR spectra, the PTh is also be doped by SO_4^{2-} derived from APS. The interaction strategy between PTh and TiO_2 proposed herein (Scheme 2) would well explain the mechanism on the synergistic adsorption between PTh and TiO_2 in the selective adsorption for heavy metals discussed in the later section.

The compounds in the composite can be also implied by the TGA analysis. The TGA curve of the PTh, TiO_2 as well as the composite before adsorption is illustrated in Fig. 1(a). The TiO_2 exhibits a two-stage thermal degradation curve; the first one at 150 °C ascribed to the elimination of the adsorbed water and the second on at 150–450 °C due to the removal of the hydroxyls on the TiO_2 [32]. While PTh and PTh/TiO_2 composite show a three-stage pyrogenic decomposition process, which situated at 150 °C ascribed to the evaporation of the adsorbed water, 150–450 °C due to the dedoping of the doping ions and over 450 °C assigned to degradation of PTh chain, respectively [33]. It can be seen that the PTh can be 98% decomposition under 800 °C, showing the lower thermo-stability of the C=O derivative PTh caused by the side chain compared with that of pure PTh [34]. This result also confirms the structure depicted in Scheme 1.

Zeta potential investigation is also carried out to get inside to the structure of the composite. The pH of zero point charge (pH_{pzpc}) of the TiO_2 is suggested as 8.41, which is reduced to 4.17 by PTh loading, as shown in Fig. 1(c). However, it should be noticed that the synthesized PTh keeps at negative charged state in the experimental range. Specifically, the PTh should keep at its doping state when it is immersed in acid solution, where positive charge and polaron can be detected [21]. In addition, the synthesized PTh cannot be n-type because n-type PTh is relatively hard to achieve due to the strict condition [20,35]. The most possible reason is the result of side chain introduced by water. The C=O group gives out more negative charges for the PTh chain. The main part of PTh should also be kept at its p-doping state before immersed into the aqueous solution, which is confirmed by the XPS study in our previous work [36].

The XRD spectra of PTh, TiO_2 and PTh/TiO_2 composite in Fig. 1 (d) also give out the detail concerning the morphology. Typical crystalline peaks at 25.3°, 37.8° and 48.1° ascribed to the anatase TiO_2 are shown in the pattern of TiO_2, while a broad peak situated at around 25° due to the π-π stacking is observed in that of PTh, confirming the pure anatase form of TiO_2 and amorphous structure of PTh [37]. The intensity of these anatase peaks decrease considerably after loading with PTh, suggesting that the TiO_2 is coating with PTh. This coating can also be confirmed by N_2 isotherm and desorption isotherm investigation shown in Fig. S2 and Table 2. The type-I shape of TiO_2 is significantly changed to type-II shape which is similar to that of PTh after coating with PTh, suggesting that the PTh shell would change the pore shape of the TiO_2 during the synthesis. From Table 2, it can be seen that the surface area and pore volume of TiO_2 is also reduced after coating, which is mainly due to the block of the PTh on the pore. SEM, TEM and TEM-EDS investigation for TiO_2 and PTh/TiO_2 composite are also carried out for the morphology, which are shown in Fig. 1(e–i) and Fig. S3. The coating of PTh around TiO_2 was clearly confirmed by the TEM-EDS images, from which a clear Ti and O core (TiO_2) can be observed to be wrapped by S and C (PTh). In addition, the size of TiO_2 increased after coating with PTh from the SEM images, further indicating the coating of PTh. From the TEM-EDS images, O element was also seen in the PTh part, further suggesting the introduction of C=O group onto the side chain of PTh using this method.

Table 2
The textural properties of the PTh, TiO_2 and PANi/TiO_2 composite before and after adsorption.

Composites	S_{BET}(m^2/g)	V(cm^3/g)	R(Å)
PTh	3.11	0.038	138.3
TiO_2	163.36	0.37	39.5
PTh/TiO_2	68.55	0.23	63.0

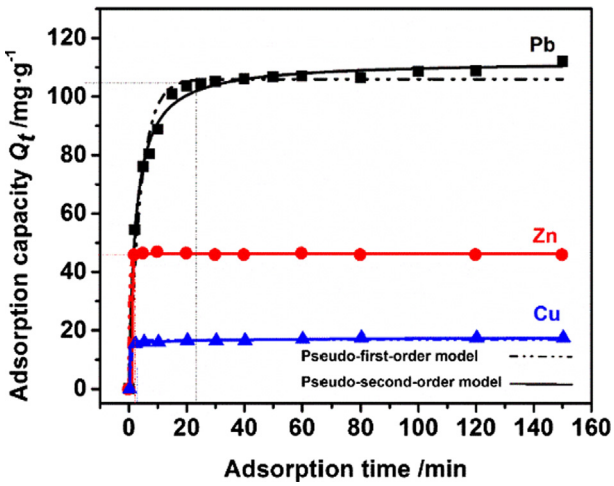

Fig. 2. Kinetic study on PTh/TiO_2 composite for Pb^{2+}, Zn^{2+} and Cu^{2+} fitted with pseudo-first-order and pseudo-second-order model.

3.2. Adsorption

3.2.1. Kinetic investigation

Equilibrium time shows the required time for removal in the adsorption procedure, which is one of the important parameters in actual application. Fig. 2 depicts the adsorption capacity in different contact time of the composite for Cu^{2+} and Zn^{2+} together with that of Pb^{2+} for comparison in a single ion system. It can be observed to be a quick process, where over 90% of the equilibrium capacity for three ions can be reached within the first 5 min for Cu^{2+} and Zn^{2+} and equilibrium time for all three ions is about 20 min. According to literatures [38,39], the quick adsorption process can be achieved by ionic doping, ionic exchange, electrostatic adsorption or chelation.

In order to know more about the adsorption pathway, the mass transfer process and the rate-limiting step, and use the model to describe and predict the adsorption process, the kinetic data are fitted with pseudo-first-order model [40], pseudo-second-order model [41] and Weber-Morris [42] model.

3.2.1.1. The pseudo-first-order model.

$$Q_t = Q_e\left(1-e^{-k_1 t}\right) \tag{3}$$

where Q_e (mg/g) and Q_t (mg/g) are the adsorption capacity at equilibrium state and at time t (min), respectively; k_1 (min^{-1}) is the rate constant of the pseudo-first-order model.

3.2.1.2. The pseudo-second-order model.

$$Q_t = \frac{Q_e^2 k_2 t}{1 + Q_e k_2 t}, \quad h = k_2 Q_e^2 \quad (t \to 0) \tag{4}$$

Where k_2 (g/(mg·min)) is the rate constant of the pseudo-second-order model; h (mg/(g·min)) is the initial adsorption rate.

The fitting parameters of the two models are listed in Table 3. The kinetic data in all cases can be better described by the pseudo-second-order model due to the higher correlation coefficient values and the closer value of the calculated capacity $Q_{e,c}$ to the experimental capacity $Q_{e,e}$. This result well suggests that the adsorption rate is controlled by the chemisorption mechanism which may relate to the ionic exchange and electron transfer [41].

3.2.1.3. Weber-Morris model.

$$Q_t = k_i t^{0.5} + C \tag{5}$$

where k_i $(mg/g/min^{0.5})$ is the rate of the intraparticle diffusion; C represents the thickness of the boundary layer. The mass transfer rate is totally controlled by the intraparticle process when $C = 0$, otherwise the liquid film transfer and intraparticle transfer govern the mass transfer rate stepwise [42].

Fig. S4 shows the plots for the three metal ions, which suggests different adsorption sites for the ions. For Zn^{2+} and Cu^{2+}, only one diffusion process involved in the adsorption, suggesting that Zn^{2+} and Cu^{2+} mainly adsorbed on the surface of the composite. For Pb^{2+}, it can be also adsorbed in the intraparticle of the composite apart from the surface. The calculated parameters of the Weber-Morris model are also listed in Table 3.

3.2.2. Selective adsorption investigation

To get insight of the selective adsorption mechanism, the PTh/ TiO_2 composite was applied in the selective adsorption investigation in single and multiple ions solution. Therefore the composite is applied for the single-ion and multi-ion isotherm investigations for Zn^{2+} and Cu^{2+}, while Pb^{2+} adsorption is redo in the single-ion isotherm and also investigated in multi-ion isotherm for comparison [43]. In the present study, the Langmuir [44] and Freundlich [45] models are applied to find the best function which can describe and predict the adsorption data well in the competition study.

3.2.2.1. The Langmuir isotherm.

$$Q_e = \frac{Q_m K_L C_e}{1 + K_L C_e} \tag{6}$$

$$P = \frac{Q_{max,single}}{Q_{max,multiple}} \tag{7}$$

$\boldsymbol{Q_e}$ (mg/g) describes the equilibrium adsorption capacity; $\boldsymbol{Q_{m,mass}}$ (mg/g)/$\boldsymbol{Q_{m,mol}}$ (mmol/g) represent the maximum adsorption capacity in different units; $\boldsymbol{K_L}$ (L/mg) is an Langmuir constant relate to the affinity between adsorbent and adsorbate; $\boldsymbol{P}$ factor is a dimensionless parameter to estimate the selectivity for heavy metals.

3.2.2.2. The Freundlich isotherm.

$$Q_e = K_F C_e^{1/n} \tag{8}$$

$\boldsymbol{K_F}$ (mg^{1-n}·L^n/g) is a constant related to the adsorption capacity of adsorbent when the equilibrium metal ions concentration equals to 1; **n** states the degree of dependence of the adsorption on the equilibrium concentration.

The isotherm data carried out in single-ion and multi-ion solution are fitted with the models as shown in Fig. 3, and the isotherm

Table 3
Kinetic parameters for the Pb^{2+}, Zn^{2+}, Cu^{2+} adsorption onto the PTh/TiO_2 composite based on the pseudo-first-order, pseudo-second-order and the Weber-Morris model.

	The pseudo-first-order model				The pseudo-second-order model					Weber-Morris model					
	$Q_{e,c}$	$Q_{e,e}$	k_1	R^2	$Q_{e,c}$	$Q_{e,e}$	k_2	h	R^2	$k_{i,1}$	C_1	R^2	$k_{i,2}$	C_2	R^2
Pb	112.0	106.63	0.243	0.967	112.0	113.38	0.0365	469.20	0.999	1.39	0.2678	0.999	16.639	36.307	0.999
Zn	46.0	46.28	2.558	0.988	46.0	45.87	0.153	322.58	0.999	53.74	0	1	–	–	–
Cu	17.5	16.79	1.269	0.987	17.5	17.64	0.045	13.93	0.999	10.96	0	1	–	–	–

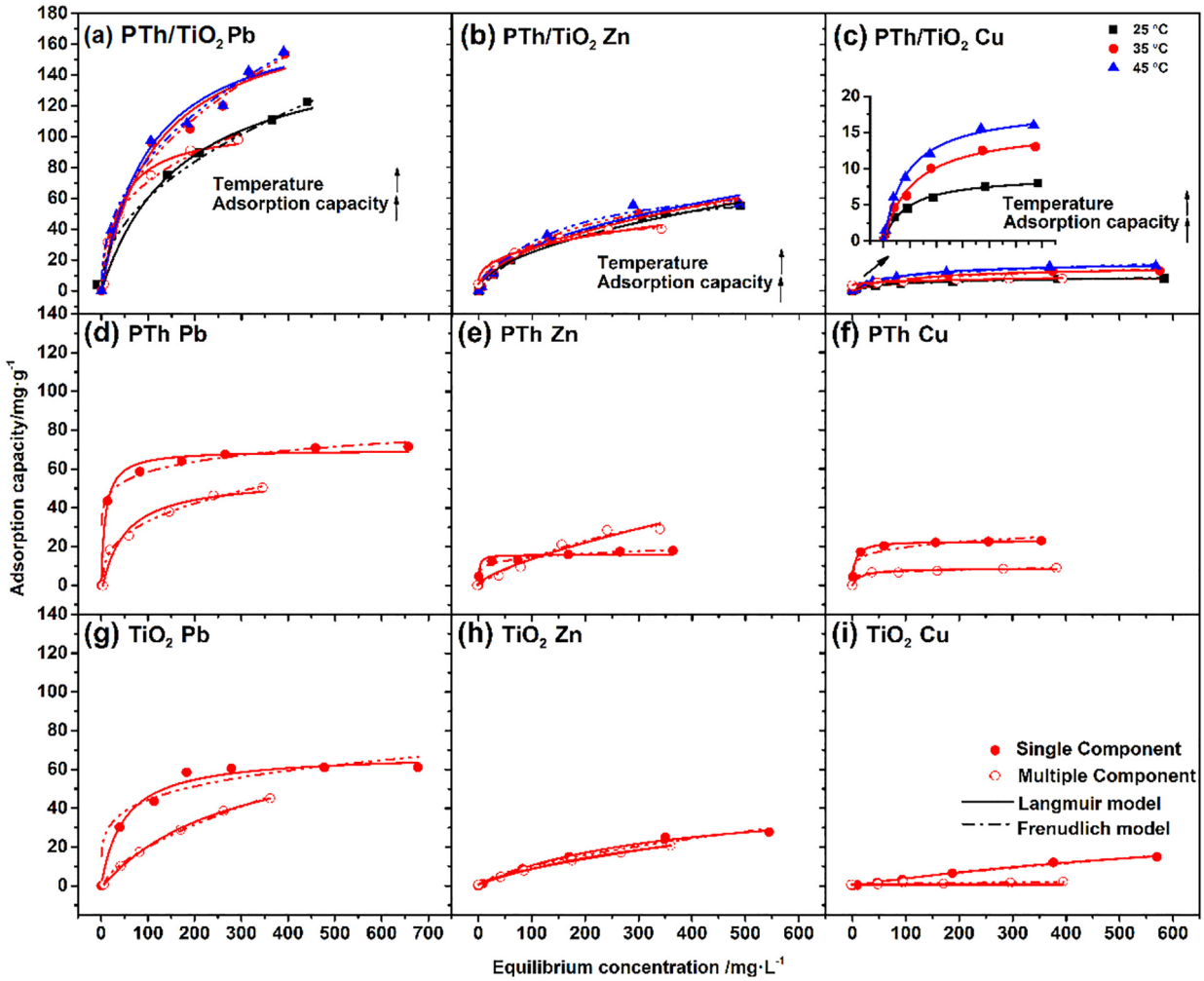

Fig. 3. Adsorption isotherms in single and multiple metal ion solution for the adsorption of Pb^{2+}, Zn^{2+} and Cu^{2+} onto PTh/TiO_2 composite (a, b, c), PTh (e, f, g) and TiO_2 (h, i, j), described with Langmuir and Freundlich model.

parameters are listed in Table 4. The high correlation coefficient values suggest that Langmuir can predict the adsorption data better in both of single-ion and multi-ion solution, indicating that the adsorption should be monolayer and homogenous [44]. The composite shows good adsorption capacity for Zn^{2+} and Pb^{2+} that reach 1.138 mmol/g and 0.79 mmol/g, while low adsorption capacity for Cu^{2+} that is 0.142 mmol/g at 25 °C. The adsorption capacity for metal ions also show a positive correlation with temperature, which is often observed in some ionic exchange and chelation adsorption [46].

To better illuminate the adsorption selectivity of the composite, the composite is also applied in the multi-ion solution for the competition study. ***P*** factor shown in Eq.(7) is introduced to correlate the data obtained from single-ion adsorption with that the multi-ion one. It can be reasonably understood that the adsorbent would have good adsorption selectivity if the difference of the ***P*** values for different metal ions are large, otherwise the adsorbent should lack adsorption selectivity. In addition, the adsorbent should have large affinity towards certain heavy metal ions if the value of ***P*** is closer to 1, otherwise it should have low affinity if the value of ***P*** is closer to 0. The ***P*** values for three heavy metals are recorded in Table 4. Encouragingly, the ***P*** values show a descending order of $Zn^{2+} > Pb^{2+} \gg Cu^{2+}$, where the adsorption of Cu^{2+} is suppressed in the competition adsorption. In addition, it can also be seen that the selectivity order of the polymer following the similar trend of TiO_2. Even though the ***P*** value of PTh also showed an obvious descending order of $Zn^{2+} > Pb^{2+} \gg Cu^{2+}$, however a positive effect of the mixture ions on the adsorption of Zn^{2+}, which is a totally different phenomenon compared with that in PTh/TiO_2 composite where the mixture ions have negative effect on the Zn^{2+} adsorption, was observed in the PTh, suggesting TiO_2 plays more important role in the selective adsorption than PTh. This makes sense because the content of PTh is only 14.16 w/w% in the PTh/TiO_2 composite according to the TGA. However, it should be addressed is PTh still play an important part in the selective adsorption of the composite because it protects the hydroxyls on the TiO_2 from combination with H^+, thus increasing the selectivity and adsorption capacity of PTh/TiO_2 composite. It should be noted that there is not a mechanism on selective adsorption that can perfectly explain all the experimental results yet, and many factors such as the cationic radius, hydration energy, Pauling electronegativity and acidity/basicity of the interactive species were applied to explain the result. However, the explanations contradict with each other in the reported literature [47–49]. Herein, another different result was acquired in this investigation that $Zn^{2+} > Pb^{2+} \gg Cu^{2+}$, even though Zn^{2+} has a smaller ionic radii and Pauling electronegativity (0.74 nm and 1.65, respectively) than Pb^{2+} (0.97 nm and 2.33, respectively) and Cu^{2+} (0.7 nm and 1.9, respectively). It indicated that the selectivity of the adsorbent majorly depends on the adsorbent and adsorbate, and the mechanism proposed before cannot well explain all these situations. A reliable mechanism should be acquired.

3.2.3. Adsorption mechanism

FT-IR analysis before and after heavy metal adsorption of the TiO_2 and PTh/TiO_2 composite shown in Fig.S1(b–c) and Table 1 was

Table 4
Single and multi-component adsorption isotherms parameters describing the adsorption of heavy metals (Pb^{2+}, Zn^{2+}, Cu^{2+}) onto the PTh/TiO_2 composite, based on Langmuir and Freundlich models.

			Samples															
			PTh/TiO_2								PTh			TiO_2				
			Pb			Zn			Cu		Pb	Zn	Cu	Pb	Zn	Cu		
			25 °C	35 °C	45 °C	25 °C	35 °C	45 °C	25 °C	35 °C	45 °C	25 °C	25 °C	25 °C	25 °C	25 °C	25 °C	25°C
Langmuir	Single-component	$Q_{m,mass}$	163.51	182.863	186.15	74.00	75.65	75.95	9.06	15.87	18.65	69.72	15.89	22.80	68.13	46.83	15.63
		$Q_{m,mol}$	0.790	0.883	0.899	1.138	1.164	1.168	0.142	0.248	0.291	0.337	0.245	0.356	0.329	0.720	0.244
		K_L	0.00584	0.00875	0.00986	0.00578	0.00642	0.00712	0.0117	0.00883	0.01128	0.112	0.571	0.190	0.020	0.0029	0.0010
		R^2	0.987	0.975	0.974	0.999	0.999	0.989	0.996	0.994	0.999	0.988	0.919	0.963	0.980	0.994	0.997
	Multi-component	$Q_{m,mass}$	–	81.43	–	–	45.91	–	–	4.06	–	55.53	64.42	8.75	45.38	45.12	0
		$Q_{m,mol}$	–	0.393	–	–	0.706	–	–	0.063	–	0.268	0.991	0.137	0.219	0.694	0
		K_L	–	0.0313	–	–	0.0125	–	–	0.01	–	0.0225	0.002	0.0649	0.0039	0.0022	–
		R^2	–	0.975	–	–	0.997	–	–	0.995	–	0.960	0.964	0.963	0.998	0.999	–
		P	**0.445**	–	–	**0.607**	–	–	**0.255**	–	–	**0.796**	**4.054**	**0.383**	**0.666**	**0.963**	**0**
Freundlich	Single-component	K_F	6.78	10.53	11.82	2.26	2.60	3.05	1.05	1.31	2.03	33.03	6.24	8.48	16.66	0.58	0.10
		$1/n$	0.475	0.446	0.429	0.522	0.508	0.487	0.327	0.375	0.337	0.124	0.183	0.183	0.21	0.62	0.80
		R^2	0.997	0.969	0.969	0.981	0.969	0.931	0.948	0.961	0.951	0.963	0.968	0.814	0.744	0.971	0.790
	Multi-component	K_F	–	11.90	–	–	3.01	–	–	0.30	–	7.18	0.51	3.71	1.15	0.30	–
		$1/n$	–	0.338	–	–	0.396	–	–	0.422	–	0.340	0.710	0.145	0.64	0.72	–
		R^2	–	0.987	–	–	0.947	–	–	0.9514	–	0.989	0.902	0.841	0.995	0.997	–

conducted for the mechanism investigation: for TiO_2, the peak ascribed to the hydroxyls at 1629 cm^{-1} shows an obvious red shift to lower wavenumbers after adsorbing Pb^{2+}, Zn^{2+} and Cu^{2+}, suggesting the hydroxyls on the surface of TiO_2 could interact with heavy metals after dedoping. However, the peak shift for Cu^{2+} is relatively smaller than the other two ions, confirming the unfavorablity of the adsorption for Cu^{2+} on TiO_2. The peak at around 1636 cm^{-1} assigned to the hydroxyls of polythiophene/TiO_2 also red-shifted to lower wavenumber after adsorbing heavy metal ions, indicating the similar interaction between composite and heavy metal ions. In the meantime, for PTh/TiO_2 composites, it can be clearly observed that the peak ascribed to C-S situated at around 652 cm^{-1} also shifts to 624, 655, and 641 cm^{-1}, respectively after Pb^{2+}, Zn^{2+}, Cu^{2+} adsorption, respectively, indicating a new circumstance around the hydroxyl on the TiO_2 and the sulfur on the PTh chain after adsorption.

An interesting self-doping structure was illuminated at the beginning that the TiO_2 which has abundant of hydroxyls on the surface would dope into the polymers as a dopant. The similar interaction between PTh and TiO_2 in PTh/TiO_2 composite was also observed by M.D Lu et al. [30] and N. Hebestreit et al [25]. However, the doping state of the PTh is even less stable than PANi and PPy from the viewpoint of electrochemistry [50]. The standard electrode potentials of water, oxygen and conducting polymers are summarized at Table 5. Specifically, when PTh is dipped in a non-acidic solution, reaction as follows will happen:

$$O_2 + H_2O + e = OH^- \quad (9)$$

$$PTh(A^-) + e = PTh^0 + A^- \quad (10)$$

$$\text{Reaction (10)} - \text{(9)}: PTh(A^-) + OH^- = PTh^0 + O_2 + H_2O + A^- \quad (11)$$

Since the difference of the electrode potentials for (9) and (10) is relatively large, the free energy of (11) is therefore large. Moreover the kinetics of this reaction is very quick according to Li et al. [50]. Therefore, the reaction still occurs very easily and thoroughly, even in a neutral solution where the concentration of the OH^- is low. For PPy and PANi, the difference between the electrode potentials is smaller, therefore they would undergo ionic exchange or partial dedoping in the non-acidic solution [50]. Thus, dedoping of SO_4^{2-} as well as $TiO_2(O^-)$ would more thoroughly occur in the $PTh^+/TiO_2(O^-)$ composite when the composite is dipped in the heavy metal ion solution where the pH = 5. This dedoping process is also confirmed by TG analysis shown in Table S1 and Fig. 1(b). It is interesting to see that in the TGA results of the composite after dipped water solution with the pH = 5, a loss of the dopant is evidently observed when compared the weight loss at the second interval with that of the composite before dipping, confirming the dedoping of the dopants. The similar trends were also observed in that of composite after ion adsorption. The unstable doping state for the PTh is also suggested by G. Tourillon et al. [51] and D. Oeter [52]. This evidence further supports the conclusion that the dedoping process of PTh occur in the heavy metal solution with pH = 5. The hydroxyl group on the TiO_2 would be influenced less and less by the shell during the

Table 5
Standard electrode potentials of water and oxygen and the electrode potentials of conducting polymers [50].

Reaction	E^0 (V vs. NHE)
$2H_2O + 2e^- = H_2 + 2OH^-$	−0.828
$O_2 + 2H_2O + 4e^- = 4OH^-$	0.414
$O_2 + 4H^+ + 4e^- = 2H_2O$	1.229
Reaction	**$E_{1/2}$ (V vs. NHE)**
$PPy(A^-) + e^- = PPy^0 + A^-$	0.023
$PPy(OH^-) + e^- = PPy^0 + OH^-$	−0.337
$PANi(A^-) + e^- = PANi^0 + A^-$	0.268
$PTh(A^-) + e^- = PTh^0 + A^-$	1.290

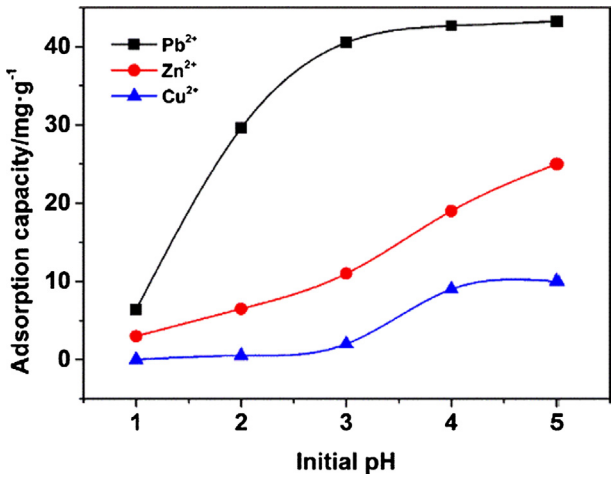

Fig. 4. Influence of initial solution pH on the adsorption capacities of PTh/TiO_2 composite for Pb^{2+}, Zn^{2+} and Cu^{2+}.

dedoping process. Therefore, the hydroxyl group on the core TiO_2 could play more important role in the selective adsorption for heavy metal ions.

By discussing the interesting dedoping properties of PTh/TiO_2 composite above, the synergistic and the selective adsorption of the composite can be well explained by following process. Specifically, the dedoping of $TiO_2(O^-)$ occurs after the composite is immersed into the heavy metal solution with the pH = 5. To keep the TiO_2 electroneutral, the positively charged heavy metal ions would be attracted and doped onto $TiO_2(O^-)$. Thus, the adsorption selectivity should be determined by TiO_2, which is clearly observed in the competition experiment. In this synergetic system, PTh plays an important part in protecting the hydroxyls on the TiO_2 from combination with H^+, thus increasing the selectivity and adsorption capacity of PTh/TiO_2 composite. The experiments by adjusting the solution pH shows that the adsorption capacities for Pb^{2+}, Zn^{2+} and Cu^{2+} increase with the pH (as shown in Fig. 4), which supports the proposed synergistic mechanism well. It is due to the reason that the dedoping process of PTh can be greatly forbidden in the acidic solution, resulting in the deterioration of the adsorption capacities for heavy metal ions. H^+ would also be adsorbed, but the competitive capacity of H^+ should be much lower than metal ions due to the low concentration of H^+ (pH = 5). We convince that the adsorption selectivity of the polymer/metal oxide should be determined by metal oxide, while polymer promote the adsorption through the dedoping process. Inspired by the doping and dedoping nature of the composite, the regeneration by using HNO_3 as the eluent agent to recycle the adsorbent was investigated and confirmed; the composite can be also employed in the simulated waste water without adsorption capacity loss (Shown in Supplementary data).

4. Conclusions

An adsorbent $PTh^+/TiO_2(O^-)$ composite with novel selective adsorption towards Zn^{2+} and Pb^{2+} with high Cu^{2+} tolerance is synthesized in aqueous medium for synergetic effect study and adsorption application. The mechanism on the selectivity of the polymer/metal oxide composites towards heavy metal ions is evidently confirmed in this paper. The coating of PTh around TiO_2 is characterized, and it suggested that the TiO_2 which has abundant of hydroxyls on the surface would be another dopant to dope into the polymer, forming an interesting self-doping heterojunction structure of $PTh^+/TiO_2(O^-)$. The unique synergistic composite shows a similar adsorption selectivity as TiO_2 that $Zn^{2+} > Pb^{2+} \gg Cu^{2+}$, where the adsorption of Cu^{2+} is suppressed in the multiple-ion solution. The composite can be thus applied in the metal ions adsorption application without the influence of Cu^{2+}. Finally, the mechanism on the novel selective adsorption is proposed with evidence. The dedoping of $TiO_2(O^-)$ from PTh due to the metastability of the doping state of PTh happens in the non-acidic solution, leading to the doping of heavy metal ions (M^{2+}) onto the $TiO_2(O^-)$ and achieving the selective adsorption finally. This encouraging mechanism could be a general guideline for adsorbent design for the adsorption engineering, by which the composite with specific adsorption selectivity can be designed and synthesized to meet specific demand in some situations. However, the mechanism on the selective adsorption on TiO_2 remains unclear. A hypothesis for the selectivity can be proposed herein that it may due to similarity of the lattice between the heavy metal oxide and TiO_2. However, it still lacks evidences to identify this hypothesis. Further work will be conducted on this aspect.

5. Supplementary data

The supplementary figures including FTIR spectra of PTh, TiO_2, PTh/TiO_2 before and after Pb^{2+}, Zn^{2+} and Cu^{2+} adsorption (Fig. S1); N_2 adsorption and desorption isotherm curves of PTh, TiO_2 and PTh/TiO_2 composite (Fig. S2); TEM images of TiO_2 and PTh/TiO_2 composite on a smaller scale (Fig. S3); multi-linear Weber-Morris model fitted curves of PTh/TiO_2 composite (Fig. S4) and the supplementary tables including the proportion of each component in PTh, TiO_2 and the PTh/TiO_2 composite before and after water or heavy metal solution treatment were supplemented (Table S1). In addition, results of adsorption experiments for application including regeneration study and field sample analysis were also shown in the Supplementary data.

Acknowledgements

The authors gratefully acknowledge Dr. Jean-Charles Eloi from Chemical Imaging Facility in University of Bristol for the SEM and TEM investigation and analysis, and Veronica Del Angel Hernandez for her kind help with the language to improve the quality of our paper. The authors also gratefully acknowledge the Shaanxi Key research and development projects, China (Grant No. 2017SF-386), the Fundamental Research Funds for the Central Universities of China and the financial supports from the National Natural Science Foundation of China (Grant No.21307098).

References

[1] Z. Xia, L. Baird, N. Zimmerman, M. Yeager, Heavy metal ion removal by thiol functionalized aluminum oxide hydroxide nanowhiskers, Appl. Surf. Sci. 416 (2017) 565–573.
[2] S. Lin, C. Lian, M. Xu, W. Zhang, L. Liu, K. Lin, Study on competitive adsorption mechanism among oxyacid-type heavy metals in co-existing system: removal of aqueous As(V), Cr(III) and As(III) using magnetic iron oxide nanoparticles (MIONPs) as adsorbents, Appl. Surf. Sci. 422 (2017) 675–681.
[3] M. Visa, C. Bogatu, A. Duta, Simultaneous adsorption of dyes and heavy metals from multicomponent solutions using fly ash, Appl. Surf. Sci. 256 (2010) 5486–5491.
[4] P. Tan, Q. Bi, Y. Hu, Z. Fang, Y. Chen, J. Cheng, Effect of the degree of oxidation and defects of graphene oxide on adsorption of Cu^{2+} from aqueous solution, Appl. Surf. Sci. 423 (2017) 1141–1151.
[5] M. Kılıç, Ç. Kırbıyık, Ö. Çepelioğullar, A.E. Pütün, Adsorption of heavy metal ions from aqueous solutions by bio-char, a by-product of pyrolysis, Appl. Surf. Sci. 283 (2013) 856–862.
[6] X. Li, Y. Liu, C. Zhang, T. Wen, L. Zhuang, X. Wang, G. Song, D. Chen, Y. Ai, T. Hayat, X. Wang, Porous Fe_2O_3 microcubes derived from metal organic frameworks for efficient elimination of organic pollutants and heavy metal ions, Chem. Eng. J. 336 (2018) 241–252.
[7] D. Alipour, A.R. Keshtkar, M.A. Moosavian, Adsorption of thorium(IV) from simulated radioactive solutions using a novel electrospun PVA/TiO_2/ZnO nanofiber adsorbent functionalized with mercapto groups: Study in single and multi-component systems, Appl. Surf. Sci. 366 (2016) 19–29.
[8] J. Maity, S.K. Ray, Chitosan based nano composite adsorbent-Synthesis, characterization and application for adsorption of binary mixtures of Pb (II) and Cd (II) from water, Carbohydr. Polym. 182 (2018) 159–171.
[9] J. Yang, J.-X. Wu, Q.-F. Lü, T.-T. Lin, Facile preparation of lignosulfonate-graphene oxide-polyaniline ternary nanocomposite as an effective adsorbent for Pb (II) Ions, ACS Sustain. Chem., Eng. 2 (2014) 1203–1211.
[10] N. Wang, J. Feng, J. Chen, J. Wang, W. Yan, Adsorption mechanism of phosphate by polyaniline/TiO_2 composite from wastewater, Chem. Eng. J. 316 (2017) 33–40.

[11] J. Chen, J. Feng, W. Yan, Influence of metal oxides on the adsorption characteristics of PPy/metal oxides for Methylene Blue, J. Colloid. Interf. Sci. 475 (2016) 26–35.
[12] J. Chen, C. Shu, N. Wang, J. Feng, H. Ma, W. Yan, Adsorbent synthesis of polypyrrole/TiO_2 for effective fluoride removal from aqueous solution for drinking water purification: adsorbent characterization and adsorption mechanism, J. Colloid. Interf. Sci. 495 (2017) 44–52.
[13] J. Li, J. Feng, W. Yan, Excellent adsorption and desorption characteristics of polypyrrole/TiO_2 composite for Methylene Blue, Appl. Surf. Sci. 279 (2013) 400–408.
[14] R.M. McKenzie, The adsorption of lead and other heavy metals on oxides of manganese and iron, Aust. J. Soil Res. 18 (1980) 61–73.
[15] J. Wu, D.A. Laird, M.L. Thompson, Sorption and desorption of copper on soil clay components, J. Environ. Qual. 28 (1999) 334–338.
[16] D.C. Adriano, Trace elements in terrestrial environments, Q. Rev. Biol. 32 (1986) 374.
[17] C. Ehrendorfer, A. Karpfen, Spatial extension of a bipolaronic defect in oligothiophenes and in polythiophene: a combined semiempirical and ab initio study, J. Phys. Chem. 98 (1994) 7492–7496.
[18] J. Guo, S. Watanabe, M.J. Janik, X. Ma, C. Song, Density functional theory study on adsorption of thiophene on TiO_2 anatase (001) surfaces, Catal. Today 149 (2010) 218–223.
[19] G. Liu, J.A. Rodriguez, J. Hrbek, B.T. Long, D.A. Chen, Interaction of thiophene with stoichiometric and reduced rutile TiO_2 (110) surfaces: role of Ti^{3+} sites in desulfurization activity, J Molecular Catal. A: Chem. 202 (2003) 215–227.
[20] J. Roncali, Conjugated poly(thiophenes): synthesis, functionalization, and applications, Chem. Rev 92 (1992) 711–738.
[21] Y. Matsuura, Y. Oshima, Y. Misaki, H. Fujiwara, K. Tanaka, T. Yamabe, S. Hotta, Synthesis and properties of oligothiophene cation radical salts, Synthetic Met. 82 (1996) 155–158.
[22] H. Chen, C.E. Nanayakkara, V.H. Grassian, Titanium dioxide photocatalysis in atmospheric chemistry, Chem. Rev. 112 (2012) 5919–5948.
[23] Y. Li, Conducting Polymers, Springer International Publishing, 2015.
[24] X. Chen, O. Inganäs, Three-step redox in polythiophenes: evidence from electrochemistry at an ultramicroelectrode, J. Phys. Chem. 100 (1996) 15202–15206.
[25] N. Hebestreit, J. Hofmann, U. Rammelt, W. Plieth, Physical and electrochemical characterization of nanocomposites formed from polythiophene and titaniumdioxide, Electrochim. Acta 48 (2003) 1779–1788.
[26] G. Zotti, Doping-level dependence of conductivity in polypyrroles and polythiophenes, Synthetic Met. 97 (1998) 267–272.
[27] A.J.W. Tol, The electronic and geometric structure of dications of oligo-thiophenes, Chem. Phys. 208 (1996) 73–79.
[28] N. Yokonuma, Y. Furukawa, M. Tasumi, M. Kuroda, J. Nakayama, Electronic absorption and Raman studies of BF^{4-}-doped polythiophene based on the spectra of the radical cation and dication of α-sexithiophene, Chem. Phys. Lett. 255 (1996) 431–436.
[29] S.S. Zade, M. Bendikov, Theoretical study of long oligothiophene dications: bipolaron vs polaron pair vs triplet state, J. Phys. Chem. B 110 (2006) 15839–15846.
[30] M.-D. Lu, S.-M. Yang, Syntheses of polythiophene and titania nanotube composites, Synthetic Met. 154 (2005) 73–76.
[31] H. Ullah, Inter-molecular interaction in Polypyrrole/TiO_2: a DFT study, J. Alloy. Compd. 692 (2017) 140–148.
[32] Y. Zhu, Z. Li, G. Chong, L. Cao, The synthesis of nanosized TiO_2 powder using a sol-gel method with $TiCl_4$ as a precursor, J. Mater. Sci. 35 (2000) 4049–4054.
[33] E.T. Kang, K.G. Neoh, K.L. Tan, Polyaniline: a polymer with many interesting intrinsic redox states, Prog. Polym. Sci. 23 (1998) 277–324.
[34] B. Singh, R.-A. Doong, D.S. Chauhan, A.K. Dubey, Anshumali, synthesis and characterization of Fe_3O_4/polythiophene hybrid nanocomposites for electroanalytical application, Mater. Chem. Phys. 205 (2018) 462–469.
[35] R.M. Crooks, O.M.R. Chyan, M.S. Wrighton, Potential dependence of the relative conductivity of poly(3-methylthiophene): electrochemical reduction in acetonitrile and liquid ammonia, Chem. Mater. 1 (1989) 2–4.
[36] J. Chen, N. Wang, H. Ma, J. Zhu, J. Feng, W. Yan, Facile modification of a polythiophene/TiO_2 composite using surfactants in an aqueous medium for an enhanced Pb(II) adsorption and mechanism investigation, J. Chem. Eng. Data 62 (2017) 2208–2221.
[37] J.C. Yu, J.G. Yu, W.K. Ho, Z.T. Jiang, L.Z. Zhang, Effects of F^- doping on the photocatalytic activity and microstructures of nanocrystalline TiO_2 powders, Chem. Mater. 14 (2002) 3808–3816.
[38] R. Karthik, S. Meenakshi, Biosorption of Pb(II) and Cd(II) ions from aqueous solution using polyaniline/chitin composite, Sep. Sci. Technol. 51 (2016) 733–742.
[39] R.-S. Norouzian, M.M. Lakouraj, Preparation and heavy metal ion adsorption behavior of novel supermagnetic nanocomposite based on thiacalix[4]arene and polyaniline: conductivity, isotherm and kinetic study, Synthetic Met. 203 (2015) 135–148.
[40] S. Lagergren, About the theory of so called adsorption of soluble substances, Kung Sven Veten Hand 24 (1898) 1–39.
[41] Y.S. Ho, Second-order kinetic model for the sorption of cadmium onto tree fern: a comparison of linear and non-linear methods, Water Res 40 (2006) 119–125.
[42] J.C. Morris, W.J. Weber, The use of adsorption for the removal of biologically-resistant pollutants from wastewaters, J. Wat. Pollut. Contro. Federa. 34 (1962) 235–236.
[43] J. Chen, J. Feng, W. Yan, Facile synthesis of a polythiophene/TiO_2 particle composite in aqueous medium and its adsorption performance for Pb(ii), RSC Adv. 5 (2015) 86945–86953.
[44] I. Langmuir, The adsorption of gases on plane surfaces of glass, mica and platinum, J. Am. Chem. Soc. 40 (1918) 1361–1403.
[45] H. Freundlich, Concerning adsorption in solutions, Zeitschrift Fur Physikalische Chemie-Stochiometrie Und Verwandtschaftslehre, 57 (1906) 385-470.
[46] M. Omraei, H. Esfandian, R. Katal, M. Ghorbani, Study of the removal of Zn (II) from aqueous solution using polypyrrole nanocomposite, Desalination 271 (2011) 248–256.
[47] S. Piri, F. Piri, B. Rajabi, S. Ebrahimi, A. Zamani, M.R. Yaftian, In situ one-pot electrochemical synthesis of aluminum oxide/polyaniline nanocomposite; characterization and its adsorption properties towards some heavy metal ions, J. Chin. Chem. Soc.-Taip. 62 (2015) 1045–1052.
[48] Q. Zhang, X. Du, X. Ma, X. Hao, G. Guan, Z. Wang, C. Xue, Z. Zhang, Z. Zuo, Facile preparation of electroactive amorphous α-ZrP/PANI hybrid film for potential-triggered adsorption of Pb^{2+} ions, J. Hazard. Mater. 289 (2015) 91–100.
[49] Z. Wang, Y. Feng, X. Hao, W. Huang, G. Guan, A. Abudula, An intelligent displacement pumping film system: a new concept for enhancing heavy metal ion removal efficiency from liquid waste, J. Hazard. Mater. 274 (2014) 436–442.
[50] Y. Li, R. Qian, Stability of conducting polymers from the electrochemical point of view, Synthetic Met. 53 (1993) 149–154.
[51] G. Tourillon, F. Garnier, Stability of conducting polythiophene and derivatives, J. Electrochem. Soc 130 (1983) 2042–2044.
[52] D. Oeter, C. Ziegler, W. Göpel, Doping and stability of ultrapure α-oligothiophene thin films, Synthetic Met. 61 (1993) 147–150.